

# PCCP

Accepted Manuscript



This is an *Accepted Manuscript*, which has been through the Royal Society of Chemistry peer review process and has been accepted for publication.

*Accepted Manuscripts* are published online shortly after acceptance, before technical editing, formatting and proof reading. Using this free service, authors can make their results available to the community, in citable form, before we publish the edited article. We will replace this *Accepted Manuscript* with the edited and formatted *Advance Article* as soon as it is available.

You can find more information about *Accepted Manuscripts* in the [Information for Authors](#).

Please note that technical editing may introduce minor changes to the text and/or graphics, which may alter content. The journal's standard [Terms & Conditions](#) and the [Ethical guidelines](#) still apply. In no event shall the Royal Society of Chemistry be held responsible for any errors or omissions in this *Accepted Manuscript* or any consequences arising from the use of any information it contains.

# High Throughput First-Principles Calculations of Bixbyite Oxides for TCO Applications

Nasrin Sarmadian,<sup>a</sup> Rolando Saniz,<sup>a</sup> Bart Partoens,<sup>a</sup> Dirk Lamoen,<sup>b</sup> Kalpana Volety,<sup>c</sup> Guido Huyberegts,<sup>c</sup> Johan Paul<sup>c</sup>

Received Xth XXXXXXXXXXXX 20XX, Accepted Xth XXXXXXXXXXXX 20XX

First published on the web Xth XXXXXXXXXXXX 200X

DOI: 10.1039/b000000x

We present a high-throughput computing scheme based on density functional theory (DFT) to generate a class of oxides and screen them with the aim of identifying those that might be electronically appropriate for transparent conducting oxide (TCO) applications. The screening criteria used are a minimum band gap to ensure sufficient transparency, a band edges alignment consistent with easy n- or p-type dopability, and a minimum thermodynamic phase stability to be experimentally synthesizable. Following this scheme we screen 23 binary and 1518 ternary bixbyite oxides in order to identify promising candidates, which can be then subject of an in-depth study. The results for the known TCOs are in good agreement with the reported data in the literature. We suggest a list of several new potential TCOs, including both n- and p-type compounds.

## 1 Introduction

Transparent conductors oxides (TCOs) have long been ubiquitous in electronic devices, and the desire of finding the optimum material for each type of application is at the heart of research efforts in the field for decades now.<sup>1</sup> Indium tin oxide,  $In_2O_3:Sn$  (ITO)<sup>1,2</sup> is one of the most widely used n-type TCOs for various optoelectronic applications. However, it does not present the optimum properties in some respects. For instance, its transparency is not as high as that of fluorine-doped ZnO.<sup>1</sup> Furthermore, because of the scarcity and high price of In, it is not cost effective, and for the past several years finding an alternative to ITO in different applications has been an important research goal for many groups. Possible routes for this include studying oxides with different structure, or substituting In partially, or replacing In altogether but still keeping the  $In_2O_3$  bixbyite structure. Of course, the number of conceivable compounds within these bounds can run into the hundreds or even thousands. Clearly, it is not possible to experimentally study all of them in order to determine whether there are other TCOs in this class of materials and whether their properties are competitive. On the other hand, high-throughput *ab initio* computations can be currently used to screen large classes of materials, searching for those compounds that exhibit a predetermined basic set of properties qualifying them as potential

competitive candidates for a certain application.<sup>3–5</sup> This approach has recently been used with success in the search for novel materials for applications ranging from field-effect transistors<sup>6</sup> to piezoelectrics<sup>7</sup> to thermoelectrics<sup>8</sup> to TCOs<sup>9</sup>.

In this work, we present the high-throughput approach schematically represented in Fig. 1, to search for candidates suitable for TCO applications. The screening criteria chosen are geared toward (i) a minimum band gap guaranteeing a reasonable transparency in the visible, (ii) a minimum thermodynamic phase stability, and (iii) a positioning of the charge neutrality level in the band gap indicating easy n- or p-type dopability. We show that this set of criteria can be efficiently used to screen the compounds in a large class of materials and that it has a good predictive power. As an application, we aim at replacing In, partially or completely, in  $In_2O_3$ . For this we screen all the binary oxides that can be found in the bixbyite structure, as well as ternaries arising from their alloying. This narrows the search to one structure, and, at the same time, increases the likelihood of finding stable compounds. We consider ternaries with cation-cation alloying ratios of 25%, 50%, and 75%. In Section 2 we present the methodology used, discussing the different stages of our approach in more detail, and in Section 3 we present our results together with a discussion. We end this work with Section 4, where we summarize our main findings.

## 2 Computational Method

Our *ab initio* computations are based on density functional theory (DFT)<sup>10,11</sup>, and are carried out using the plane-wave

<sup>a</sup> CMT, Departement Fysica, Universiteit Antwerpen, Groenenborgerlaan 171, B-2020 Antwerpen, Belgium. Fax: 32-3-2653542; Tel: 32-3-2653439; E-mail: nasrin.sarmadian@uantwerp.be

<sup>b</sup> EMAT, Departement Fysica, Universiteit Antwerpen, Groenenborgerlaan 171, B-2020 Antwerpen, Belgium. Fax: 32-3-2653542; Tel: 32-3-2653439.

<sup>c</sup> Flamac, a division of SIM, Technologiepark 903, 9052 Zwijnaarde, Belgium.

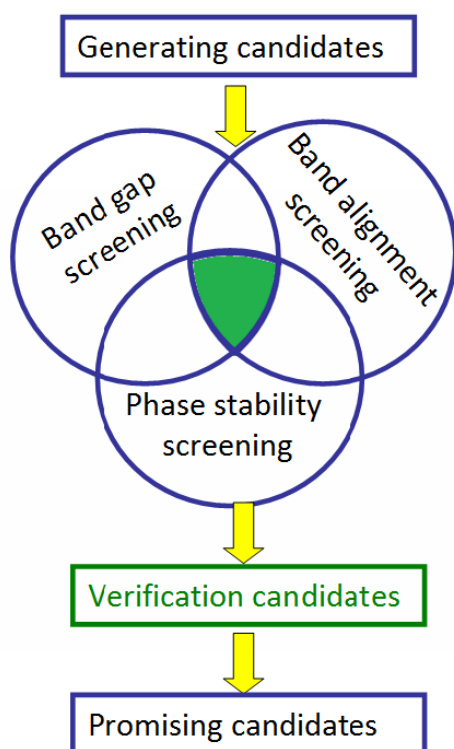


**Fig. 1** The high throughput screening procedure to identify new promising TCO candidates among bixbyite oxides.

Vienna Ab-initio Simulation Package (VASP).<sup>12–15</sup> We use projector augmented wave (PAW)<sup>16,17</sup> potentials to describe the electron-ion interaction. We use the Perdew, Burke, and Ernzerhof (PBE)<sup>18</sup> generalized gradient approximation (GGA) to the exchange-correlation potential to perform all structural calculations. Formation energies and electronic structure are calculated using either the PBE functional, or the Heyd, Scuseria, Ernzerhof (HSE06) hybrid functional.<sup>19,20</sup> In general the HSE functional improves the band gap compared to PBE for bulk semiconductors.<sup>21</sup> It is, however, much more costly from a computational point of view, and cannot be used systematically in a high-throughput approach. We use it, thus, selectively, as explained in more detail further down, to calculate the properties of all the binary oxides, and to confirm the properties of several of the more promising ternary oxides. The bixbyite structure is a cubic structure. its primitive cell (space group  $Ia\bar{3}$ , No. 206) contains 8 formula units, i.e., 40 atoms (cf. Fig. 3). An energy cutoff of 520 eV was used for the plane-wave basis set. Total energies were converged to within 1 meV. This was achieved using  $3 \times 3 \times 3$  Monkhorst-Pack (MP) grid to sample the Brillouin Zone.<sup>22</sup> Atomic relaxations were made until residual forces on the atoms were less than 0.01 eV/Å.

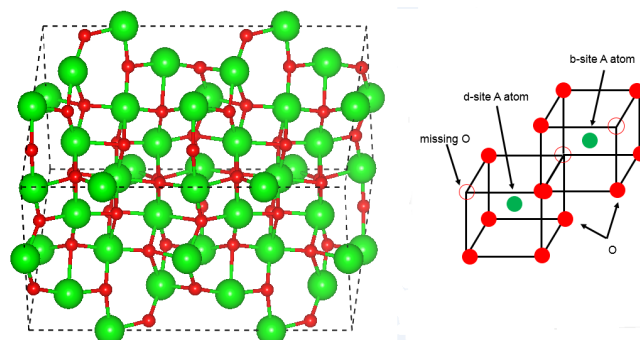


**Fig. 2** *Left*: Example of a  $A_2O_3$  bixbyite 40-atom unit cell. The red color indicates oxygen atoms. *Right*: Schematic illustration of the atomic arrangement around cation A in Wyckoff sites *b* and *d*. The oxygen atoms are denoted by solid red circles, the A atoms by green circles, and the missing oxygen atoms (with respect to the parent rocksalt structure) by open circles.

## 2.1 Generating candidates

As seen in Fig. 1, we first generate the candidates to be screened. To begin, we consider all the binary bixbyite oxides reported to exist in the literature. These have the formula  $A_2O_3$ , with A belonging to the set  $\mathcal{S} = \{\text{Sc, V, Mn, Fe, Ga, Y, In, La, Ce, Pr, Pm, Sm, Eu, Gd, Tb, Dy, Ho, Er, Tm, Yb, Lu, Tl, Bi}\}$ . We then combine two such oxides to construct ternary oxides. These are bixbyite oxides with general formula  $(A_{1-x}B_x)_2O_3$ , with A and B belonging to  $\mathcal{S}$ . In the present study,  $x$  takes the values 0, 0.25, 0.50, and 0.75. This should be sufficient to observe trends in the properties of interest as a function of alloying concentration. The bixbyite structure can be seen as the  $MnO_2$  fluorite structure, with one fourth of the O atoms removed. As shown in Fig. 2, the A atoms in  $A_2O_3$  occupy two inequivalent Wyckoff sites, *b* (site symmetry  $S_6$ ) and *d* (site symmetry  $C_2$ ), with a distorted octahedral coordination of O atoms. Four of the A atoms in the bixbyite structure sit in *b* sites, and 12 occupy *d* sites. As a result, there are different possible configurations for every alloying concentration. Again, to detect trends we choose randomly some of the possible configurations. We verify that different possible configurations lead essentially to the same conclusions in the case of 50% alloying, i.e.,  $x=0.5$ , in which case we consider four possible configurations. For the 25% and 75% alloying compounds we consider at random one possible configuration. Thus, in this study we screen the electronic properties of a total of 1541 bixbyite oxides (23 binary and 1518 ternary oxides).

## 2.2 Band gap screening

One of the most important properties of a TCO is its band gap value. A good TCO needs a large enough band gap (of the

order of 3 eV) to be transparent in the visible light range.<sup>23</sup> To screen the generated compounds according to this property, we calculate *ab initio* their band gaps. In this regard, it is known that standard DFT calculations, using local or semi-local exchange-correlation functionals such as the LDA or PBE, seriously underestimate the band gap of the semiconductors,<sup>24,25</sup> while the hybrid functional HSE06 has proven to be capable of giving close-to-experiment predictions for a large range of compounds.<sup>26</sup> Because of its computational cost, however, we rely on the HSE06 functional to calculate the band gap of only the binary oxides, which constitute a relatively small subset of all the oxides we consider. We choose to screen out the binaries with a band gap smaller than 2.5 eV. For the ternary oxides, we follow two approaches. In the first approach, we use the PBE functional, screening out the ternaries with a band gap energy lower than 1 eV. This is because a material predicted to have a band gap of 1 eV with the PBE functional might in fact have an experimental band gap closer to the requirement for a good TCO. We verify this with the HSE06 functional for candidate oxides that have successfully passed the three screening criteria in our procedure. In the second approach, we interpolate the HSE06 band gaps of the binary oxides to obtain an estimate of the band gaps of the ternaries. Again, we screen out those with a band gap energy below 2.5 eV. We note that, to be consistent, we follow the same two approaches in the band alignment and phase stability screening steps discussed below. That is, on one hand we calculate the relevant quantities using the PBE functional, and on the other, we interpolate the HSE06 results for the binaries.

### 2.3 Band alignment screening

In this step, we screen the candidate materials searching for those that can be expected to be easily *n*- or *p*-type dopable. A good predictor for this purpose is to see the alignment of the conduction band minimum (CBM) and valence band maximum (VBM) of a material with respect to the branch-point energy (BPE).<sup>27</sup> Indeed, if the BPE falls high up in the band gap, or above the CBM in a material, it is a good indication that the material will be easily doped *n*-type. Conversely, if the BPE falls low in the band gap, or below the VBM, then the material is probably easily *p*-type dopable. The BPE can be calculated as a weighted average of the midgap energies over the Brillouin zone,<sup>28,29</sup>

$$E_{BP} = \frac{1}{2N_k} \sum \left[ \frac{1}{N_{CB}} \sum_i \varepsilon_{c_i}(k) + \frac{1}{N_{VB}} \sum_j \varepsilon_{v_j}(k) \right]. \quad (1)$$

Here,  $N_k$  is the number of points in the *k*-point mesh,  $N_{CB}$  and  $N_{VB}$  are the number of conduction and valence bands considered, with  $\varepsilon_c$  and  $\varepsilon_v$  their corresponding energies. The number of valence and conduction bands used is determined by

scaling them according to the number of valence electrons in the primitive cell (excluding *d* electrons), as in the work of Schleife *et al.*<sup>28</sup> We checked that a  $3 \times 3 \times 3$  *k*point mesh is sufficient to give a converged BPE value.

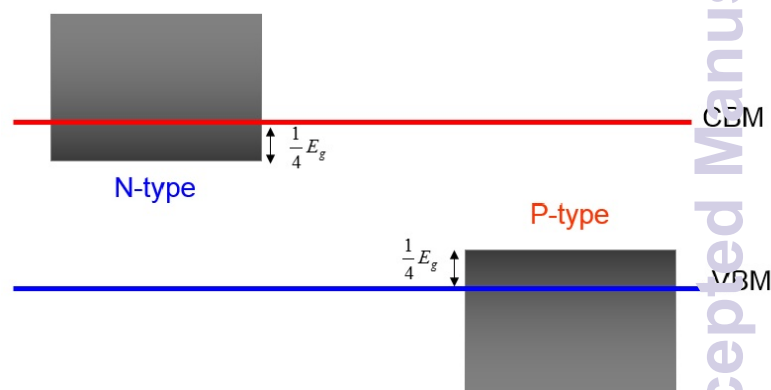


**Fig. 3** Schematic band alignment. The gray shaded area represents the accepted BPE position with respect to the CBM (*n*-type) or VBM (*p*-type) in our screening procedure.

Figure 3 illustrates our screening criterion regarding dopability. The oxides for which the BPE falls in the conduction band or in the upper part of the band gap, within at least one-fourth of  $E_g$  below the CBM (cf. shaded area at the left in Fig. 3), are considered as *n*-type oxides. Conversely, the oxides for which the BPE falls in the valence band, or maximum one-fourth of  $E_g$  above the VBM are considered as *p*-type oxides (cf. shaded area on the right side in Fig. 3).

### 2.4 Phase stability screening

A new candidate should be thermodynamically stable. Thus, one of our screening criteria is the phase stability of the candidates. Since all the binary oxides considered here have been synthesized, we focus on the ternary oxides. The formation energies of ternary oxides depend on the chemical potentials of the different constituent elements ( $\mu_A$ ,  $\mu_B$ , and  $\mu_O$ ). The chemical potentials depend on the experimental growth conditions of the compound which can vary from X-poor to X-rich, where X could be either of A, B or O. For a considered ternary oxide  $(A_xB_{1-x})_2O_3$  the formation energy is given by:

$$\Delta H_f^{(A_xB_{1-x})_2O_3} = 2x\Delta\mu_A + 2(1-x)\Delta\mu_B + 3\Delta\mu_O \quad (2)$$

where  $\Delta\mu_{A/B} = \mu_{A/B} - \mu_{A/B}^{(A/B)bulk}$ , and  $\Delta\mu_O = \mu_O - \mu_O^{O_2molecule}$ .

There should be a minimum range of possible values for these chemical potentials ensuring a stable oxide against the

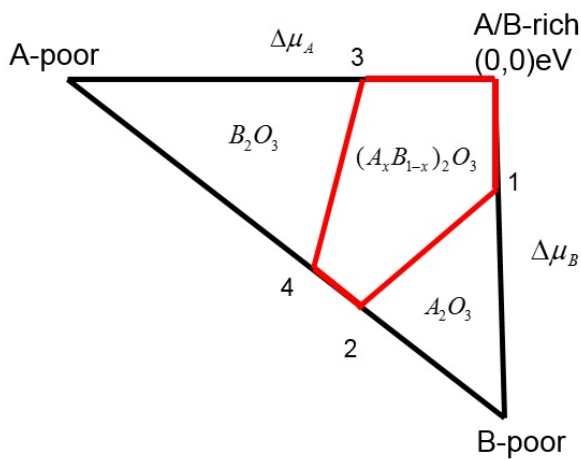


**Fig. 4** Schematic stability triangle. The area inside the red contour indicates the range of chemical potentials for which the bixbyite ternary oxide is stable against the formation of the competing phases indicated.

formation of the binary phases or precipitation of the constituent elements:

$$\Delta\mu_A \leq 0, \Delta\mu_B \leq 0, \Delta\mu_O \leq 0 \quad (3)$$

The range of the chemical potentials determined by the heat of formation of the oxide and the limitation imposed by avoiding the precipitation of the constituent elements can be plotted in a two-dimensional graph, resulting in what is known as the stability triangle in the literature.<sup>30,31</sup> This is schematically shown in a two-dimensional ( $\mu_A$ ,  $\mu_B$ ) plane in Fig. 4. The vertices of the stability triangle are given by the host condition Eq. 2 giving the limits of A/B rich, A-poor, and B-poor environments, respectively. The A-rich condition ( $\Delta\mu_A = 0$ ) leads to the maximum possible variation of the B chemical potential  $\Delta\mu_B = \frac{1}{2(1-x)}\Delta H_f^{(A_xB_{1-x})_2O_3}(\Delta\mu_O = 0)$ . On the other hand, the B-rich condition ( $\Delta\mu_B = 0$ ) leads to  $\Delta\mu_A = \frac{1}{2x}\Delta H_f^{(A_xB_{1-x})_2O_3}$ . The line joining the A-poor and B-poor vertex refers to  $\Delta\mu_O = 0$  and mimics the oxygen rich condition. Thus within this triangle the ternary oxide can exist, but the binary structures might have a lower formation energy. Therefore, the constraints are also imposed by the formation of competing binary oxides  $A_2O_3$ , and  $B_2O_3$  which are

$$2\Delta\mu_{A/B} + 3\Delta\mu_O \leq \Delta H_f^{(A/B)_2O_3} \quad (4)$$

These constraints limit the possible accessible range of chemical potentials ( $\Delta\mu_{A/B}$ ) for  $(A_xB_{1-x})_2O_3$ . The vertices of this stable region are labeled as (1,2,3,4) and the coordinates of the vertices are given by ( $\Delta\mu_A$ ,  $\Delta\mu_B$ ,  $\Delta\mu_O$ ) which can be determined as follows. The first vertex, (1), refers to A-rich conditions ( $\Delta\mu_A = 0$ ) which leads to  $\Delta\mu_O = \frac{1}{3}\Delta H_f^{A_2O_3}$  and

$\Delta\mu_B = \frac{1}{2(1-x)}(\Delta H_f^{(A_xB_{1-x})_2O_3} - \Delta H_f^{A_2O_3})$  by using Eqs. 4 and 2 respectively. Second and fourth vertices, (2), and (4), refer to O-rich conditions ( $\Delta\mu_O = 0$ ). For vertex (2) the O-rich condition should be applied in Eq. 3 under the condition that  $A_2O_3$  is formed, which leads to  $\Delta\mu_A = \frac{1}{2}\Delta H_f^{A_2O_3}$ . Inserting this value into Eq. 2 yields  $\Delta\mu_B = \frac{1}{2(1-x)}(\Delta H_f^{(A_xB_{1-x})_2O_3} - x\Delta H_f^{A_2O_3})$ . For vertex (4) a similar analysis can be made but now with the formation of  $B_2O_3$ , which results in  $\Delta\mu_B = \frac{1}{2}\Delta H_f^{B_2O_3}$  and  $\Delta\mu_A = \frac{1}{2x}(\Delta H_f^{(A_xB_{1-x})_2O_3} - (1-x)\Delta H_f^{B_2O_3})$ . Vertex (3) refers to B-rich conditions ( $\Delta\mu_B = 0$ ) which yields  $\Delta\mu_O = \frac{1}{3}\Delta H_f^{B_2O_3}$  and  $\Delta\mu_A = \frac{1}{2x}(\Delta H_f^{(A_xB_{1-x})_2O_3} - \Delta H_f^{B_2O_3})$  on applying Eqs. 4 and 2 respectively.

The relative size of the stable region with respect to the total area of the triangle shows how easy or how difficult it is to realize the thermodynamic conditions under which  $(A_xB_{1-x})_2O_3$  formation can take place and the precipitation of the parent binary compounds can be avoided. In order to limit the list of potential TCOs we impose a minimum ratio of 10% between the area of the stability region and that of the whole triangle.

## 3 Results

### 3.1 Binary oxides

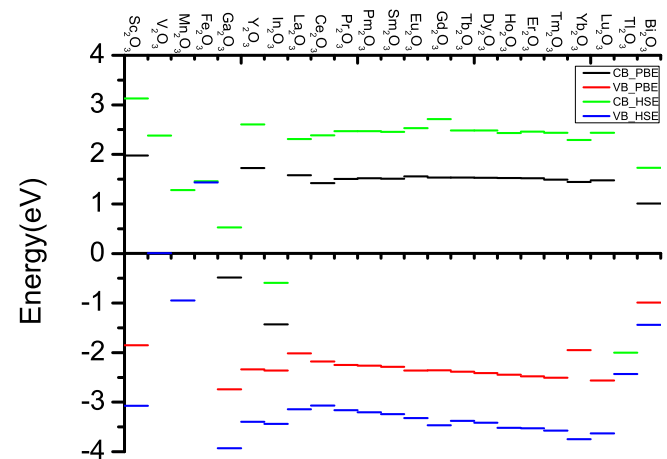


**Fig. 5** The band alignment of binary oxides, comparing the positions of the CBM and VBM calculated using the PBE and HSE06 functionals. The band edges are aligned with respect to the BPE.<sup>a</sup>

We consider first the binary oxides,  $A_2O_3$ . For these materials, we calculate lattice parameters, band gaps, and forma-

<sup>a</sup> For the materials that PBE describes as metallic, only HSE results are shown. These materials include  $V_2O_5$ ,  $Mn_2O_3$ ,  $Fe_2O_3$ , and  $Tl_2O_3$ .

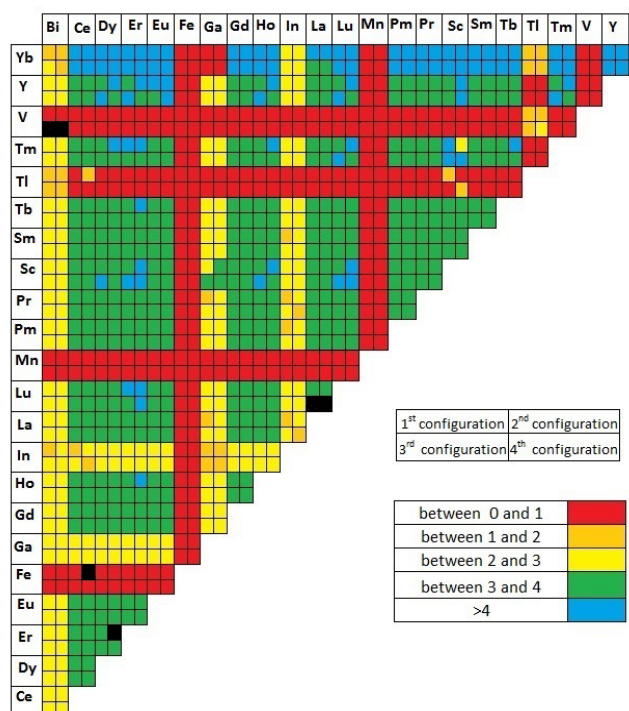


**Fig. 6** PBE band gap for the 50% ternary compounds. The cells for each pair of cations are subdivided in four subcells, corresponding to the four possible configurations considered.

tion energies using both the PBE and HSE06 functionals. In addition, we calculate the electron or hole effective masses, according to whether the band alignment indicates good electron or hole dopability. This is of particular interest to TCOs because mobility, a key quantity for the efficiency of many electronic devices, is inversely proportional to the electron effective mass. The effective mass is calculated along the  $\Gamma - X$  direction. This is sufficient because the bixbyite are cubic systems, so the effective mass is isotropic. In the first instance, we use the PBE functional for this calculation because it is known to give good values for the effective mass of semiconductors compared to experiment. However, when the PBE wrongly predicts a binary to be a metal, we use the HSE06 functional to estimate the effective mass.

Table 1 shows our results for the lattice constant, band gap (determined with the HSE06 hybrid functional), and effective mass of the binary oxides. For comparison, experimental data and/or other theoretical results are shown where available.<sup>a</sup>

<sup>a</sup>The experimental or theoretical method is also indicated when available. The theoretical gap values refer to the fundamental band gap.

**Table 1** Comparing our calculated lattice constant, band gap, and effective mass (in units of the free electron mass  $m_0$ ) for the binary oxides with experiment and other theoretical results.

Binary oxide	a(Å)	$E_g$ (eV)	$m^*$	$\Delta_f H$ (eV)	reference
Sc <sub>2</sub> O <sub>3</sub>	9.915	6.205	1.143	-17.80	this work
	9.50	6 <sup>b</sup>			Y. Bréard et al. <sup>32††</sup>
					H. H. Tippins. <sup>33§</sup>
	9.911				J. R. Rustad. <sup>34†</sup>
			-19.78	CRC <sup>35†</sup>	
V <sub>2</sub> O <sub>3</sub>	9.263	2.388	6.807 <sup>a</sup>	-10.43	this work
	9.3947				D. Weber et al. <sup>36††</sup>
		1.29 <sup>b</sup>			A. Bergerud et al. <sup>37£</sup>
Mn <sub>2</sub> O <sub>3</sub>	9.034	2.422	2.422	-7.00	this work
	9.41				C.M. Julien et al. <sup>38††</sup>
Fe <sub>2</sub> O <sub>3</sub>	8.977	0.026		-5.28	this work
	9.5				Y. Bréard et al. <sup>32††</sup>
	9.393				L. Ben-Dor et al. <sup>39††</sup>
Ga <sub>2</sub> O <sub>3</sub>	9.409	4.455	0.225	-13.26	this work
	9.401	2.3			S. Yoshioka et al. <sup>40†</sup>
Y <sub>2</sub> O <sub>3</sub>	10.705	5.999	0.516	-17.88	this work
	10.637				Ž. Antić et al. <sup>41††</sup>
		6			P. W. Peacock et al. <sup>42#</sup>
		6.2			G. Wilk et al. <sup>43</sup>
	10.701				J. R. Rustad. <sup>34†</sup>
				L. Marsella et al. <sup>44†</sup>	
				-19.74	CRC <sup>35†</sup>
In <sub>2</sub> O <sub>3</sub>	10.305	2.849	0.166	-9.05	this work
	10.10				A. Bourlange et al. <sup>45††</sup>
		2.9 <sup>c</sup>			A. Walsh et al. <sup>46§</sup>
		2.93 <sup>c</sup>			P. D. C. King et al. <sup>47§</sup>
	10.33				I. Tanaka et al. <sup>48†</sup>
		2.67		S. Lany et al. <sup>490</sup>	
				-9.59	CRC <sup>35†</sup>
La <sub>2</sub> O <sub>3</sub>	11.375	5.451	0.685	-18.63	this work
	11.136				G.-Y. Adachi. <sup>50††</sup>
		4			L. Marsella et al. <sup>44†</sup>
	11.387				J. R. Rustad. <sup>34†</sup>
		5.7		G. Wilk et al. <sup>43</sup>	
				-18.59	CRC <sup>35†</sup>
Ce <sub>2</sub> O <sub>3</sub>	11.405	5.454	1.136	-19.74	this work
	11.16				G.-Y. Adachi. <sup>50††</sup>
	11.414				J. R. Rustad. <sup>34◇</sup>
Pr <sub>2</sub> O <sub>3</sub>	11.180	5.632	0.528	-16.74	this work
	11.52				G.-Y. Adachi. <sup>50††</sup>
	11.290				J. R. Rustad. <sup>34†</sup>
Pm <sub>2</sub> O <sub>3</sub>	11.071	5.673	0.508	-30.05	this work
	10.99				G.-Y. Adachi. <sup>50††</sup>
Sm <sub>2</sub> O <sub>3</sub>	11.000	5.697	0.495	-17.34	this work
	10.93				G.-Y. Adachi. <sup>50††</sup>
		5.04			A. F. Andreeva et al. <sup>51</sup>

Table1 Continued

Binary Oxide	a(Å)	E <sub>g</sub> (eV)	m*	Δ <sub>f</sub> H(eV)	reference
Eu <sub>2</sub> O <sub>3</sub>	10.998	4.4	0.488	-18.89	J. R. Rustad. <sup>34†</sup>
	10.805				H. Jiang et al. <sup>52‡</sup>
	10.866				CRC <sup>35‡</sup>
Gd <sub>2</sub> O <sub>3</sub>	10.814	5.851	0.479	-18.80	this work
	10.813				G.-Y. Adachi. <sup>50††</sup>
	10.819				M. Badylevich et al. <sup>55  </sup>
Tb <sub>2</sub> O <sub>3</sub>	10.741	5.860	0.470	-22.67	this work
	10.730				G.-Y. Adachi. <sup>50††</sup>
	10.744				A. F. Andreeva et al. <sup>51</sup>
Dy <sub>2</sub> O <sub>3</sub>	10.676	5.895	0.432	-18.07	this work
	10.667				G.-Y. Adachi. <sup>50††</sup>
	10.675				A. I. Shelykh et al. <sup>56</sup>
Ho <sub>2</sub> O <sub>3</sub>	10.605	5.952	0.451	-18.30	this work
	10.607				G.-Y. Adachi. <sup>50††</sup>
	10.609				A. I. Shelykh et al. <sup>56</sup>
Er <sub>2</sub> O <sub>3</sub>	10.533	5.980	0.444	-18.29	this work
	10.547				G.-Y. Adachi. <sup>50††</sup>
	10.544				A. I. Shelykh et al. <sup>56</sup>
Tm <sub>2</sub> O <sub>3</sub>	10.472	6.011	0.431	-18.46	this work
	10.488				A. W. Carbonari et al. <sup>57‡</sup>
	10.472				A. I. Shelykh et al. <sup>56</sup>
Yb <sub>2</sub> O <sub>3</sub>	10.682	6.038	0.474	-11.19	this work
	10.439				G.-Y. Adachi. <sup>50††</sup>
					A. F. Andreeva et al. <sup>51</sup>
				-18.81	CRC <sup>35‡</sup>

Table1 Continued

Binary Oxide	a(Å)	E <sub>g</sub> (eV)	m*	Δ <sub>f</sub> H(eV)	reference
Lu <sub>2</sub> O <sub>3</sub>	10.360	6.066	0.419	-18.63	this work
	10.438				Ž. Antić et al. <sup>41††</sup>
	10.391				G.-Y. Adachi. <sup>50††</sup>
		5.5			A. I. Shelykh et al. <sup>56</sup>
		4.5			H. Jiang et al. <sup>52‡</sup>
				-19.46	CRC <sup>35†</sup>
Tl <sub>2</sub> O <sub>3</sub>	10.766	0.431	0.119 <sup>a</sup>	-3.57	this work
	10.541				A. W. Carbonari et al. <sup>54‡</sup>
	10.56	0.33			A. B. Kehoe et al. <sup>58∅</sup>
Bi <sub>2</sub> O <sub>3</sub>	11.217	3.169	36.776	-10.18	this work
	11.21				A. Matsumoto et al. <sup>59†</sup>

<sup>a</sup>m\* is the calculated effective mass of the hole.

<sup>b</sup> optical band gap

<sup>c</sup> fundamental band gap

† GGA

‡ LDA + scissors correction

◇ LDA+U

‡ G<sub>0</sub>W<sub>0</sub>@LDA + U

(Fundamental band gaps are estimated from Fig. 3 in Ref. 52)

∅ HSE06

†† X-ray powder diffraction

§ UV absorption spectroscopy

£ UV-visible spectroscopy

|| photoconductivity

§ X-ray photoemission spectroscopy

† very low pressure reactor technique

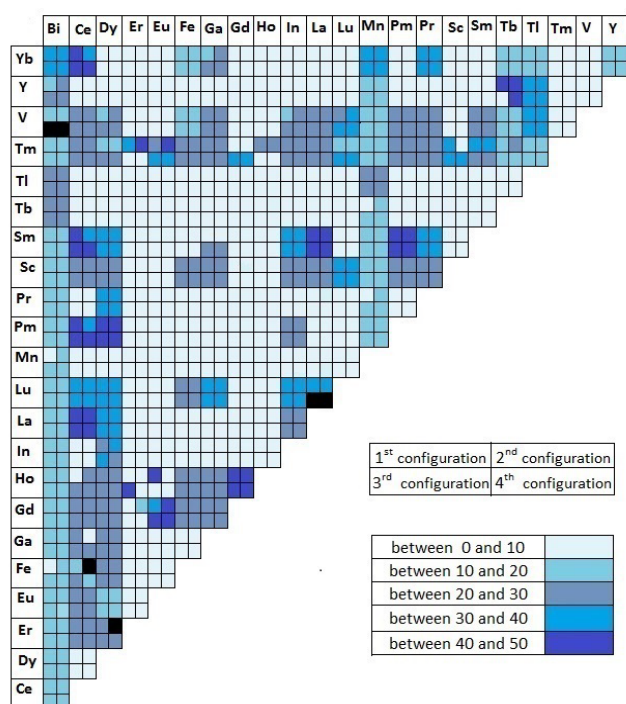


**Fig. 7** PBE calculated percent of the stability area of the 50% ternary compounds with respect to the total area of the stability triangle. The cells are subdivided as in Fig. 6.

Note that for the transition metal oxides, such as  $Y_2O_3$  and  $Sc_2O_3$ , the calculated band gaps are in very good agreement with experiment. On the other hand, the band gap of the lanthanides is systematically overestimated. This does not affect the outcome of our screening procedure, since it only involves a lower limit for the band gap and not an upper limit. We calculate, furthermore, the standard enthalpy of formation energy of all the studied binary oxides ( $A_2O_3$ ), i.e., taking as reference the energies of the constituent elements in their standard states (oxygen molecule for O and crystalline solid for A). The results, also presented in Table 1, show that all studied binary oxides are stable, as expected. For comparison, where available, the experimental values are also shown.

Fig. 5 shows the band alignment for the studied binary oxides, where the positions of CBM and VBM with respect to their BPEs are indicated. The results using both the PBE and HSE06 functionals are shown. For  $In_2O_3$ , the calculated band gap and the positions of CBM and VBM are in good agreement with experimental and other theoretical results<sup>47</sup>. The position of the BPE in  $In_2O_3$ , above the CBM, indicates that it should be readily doped *n*-type, while doping it *p*-type should be more difficult, which is indeed a well known experimental fact.<sup>60</sup> Fig. 5 also shows that  $Ga_2O_3$  in its bixbyite structure is a good *n*-type TCO candidate. It is interesting to note that

$Ga_2O_3$  in its monoclinic phase ( $\beta - Ga_2O_3$ ) has a band gap of 4.9 eV and exhibits *n*-type conductivity.<sup>61</sup> Furthermore, one can see in Fig. 5 that bixbyite  $V_2O_3$ , with a band gap of 2.4 eV, is an interesting candidate material for a *p*-type TCO. In its corundum ground state structure  $V_2O_3$  is a metal. The structural phase transition from corundum to monoclinic occurs at 170 K.<sup>62</sup> In its monoclinic phase  $V_2O_3$  is an antiferromagnetic insulator with a band gap of 0.6 eV.<sup>63</sup> The study of  $V_2O_3$  is mostly limited to its metal-insulator transition. However, vanadium sesquioxide was recently synthesized in the bixbyite structure,<sup>36</sup> and several of its basic properties have now been reported.<sup>37,64</sup>

### 3.2 Ternary oxides

We calculate the formation energy, lattice parameter, band gap, and positions of the band edges of the ternary compounds generated as indicated above. The calculations are done with the PBE functional in our first approach (cf. Section 2.2). As mentioned, there are several possible configurations for a given alloying percentage. To see the effect of configuration on the properties of interest, we study the  $(A_{0.5}B_{0.5})_2O_3$  compounds. An analysis of the formation energies shows that 9%, 45%, 31%, and 13% of these oxides prefer the 1st, 2nd, 3rd, and 4th configurations considered, respectively. The difference between the lattice parameter of two comparing configurations is smaller than 5%. More importantly, the difference in the formation energies between two different configurations of more than 91% of the 50% ternaries, is smaller than 5%. This indicates that the configuration has a small effect on the stability triangle. Also, we find that for more than 95% of the 50% ternary oxides, the difference between the band gap of two different configurations is smaller than 10%. The configuration has a similarly weak effect on band alignment. Thus, we consider that including all possible configurations in this study would not alter significantly our conclusions. Figures 6 and 7 illustrate the capability of high-throughput calculations, where band gap (Fig. 6) and stability triangle (Fig. 7) of the 50% alloys (253 oxides) are screened. The different colors indicate how close or far the different oxides are to fulfill the screening criteria. There are four boxes for each oxide, representing the four different configurations considered. Black boxes indicate the very few cases in which the calculations failed to converge.

To analyze the effect of alloying concentration on the band gap and lattice constant, we compare the calculated values with those obtained using Vegard's law<sup>65</sup>. For the lattice constant, the latter predicts

$$a_{A_{1-x}B_x} = xa_A + (1-x)a_B. \quad (5)$$

The analysis of the results shows that the Vegard's law is satisfied by most of the ternary oxides considered. Indeed, for more than 91% of all four configurations of the 50% alloys the

difference between the calculated lattice parameter and the interpolated value using Vegard's law is smaller than 5%. This is also the case for 98% of the 25%  $[A_{0.75}B_{0.25}]_2O_3$  and 75%  $[A_{0.25}B_{0.75}]_2O_3$  alloys. A similar comparison for the band gaps shows that for most of the studied ternary compounds, the deviation of the calculated band gap from Vegard's law is smaller than 10%. The difference is large only in the cases in which one of the binary oxides is wrongly predicted to be a metal by the PBE functional (namely,  $A=Fe, Mn, Tl, \text{ and } V$ ). But, of course, in such cases Vegard's law cannot be applied to the band gap.

As indicated in the section devoted to computational aspects, in addition to the calculations based on the PBE functional, we estimate the band gaps, band alignment, and phase stability area for the ternaries by interpolating the HSE06 results for the binaries. The relatively good compliance with Vegard's law of the lattice parameter and band gap as a function of alloying concentration, already mentioned above, supports this approach.

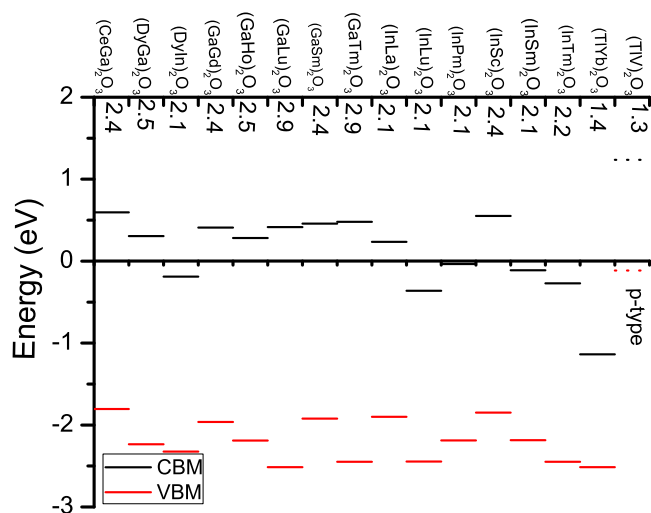


**Fig. 8** PBE band alignment of the most stable configuration of the 50% ternary compounds.<sup>a</sup>

By screening properties of the 1518 ternary oxides we generated and by discarding the oxides which do not fulfill the three criteria we impose, we find a list of candidate TCOs.<sup>b</sup> The calculations predict these to have band gap larger than 1 eV,  $n$ - or  $p$ -type band alignment, and a stability region in the stability triangle larger than 10%, and a band gap larger

<sup>a</sup>Thus, for instance,  $(Bi_{0.5}Ce_{0.5})_2O_3$  is a  $n$ -type TCO candidate in its 1st configuration, but that is not its most stable one among the four considered configurations, so it is not included in Fig. 8. In the case of  $(Tl_{0.5}V_{0.5})_2O_3$ , a  $p$ -type TCO candidate, the 3rd configuration is the most stable one.

<sup>b</sup>All calculated data are available as electronic supplementary information.

<sup>c</sup>As indicated before, for the 25% and 75% compounds, one of the possible configurations is chosen at random.

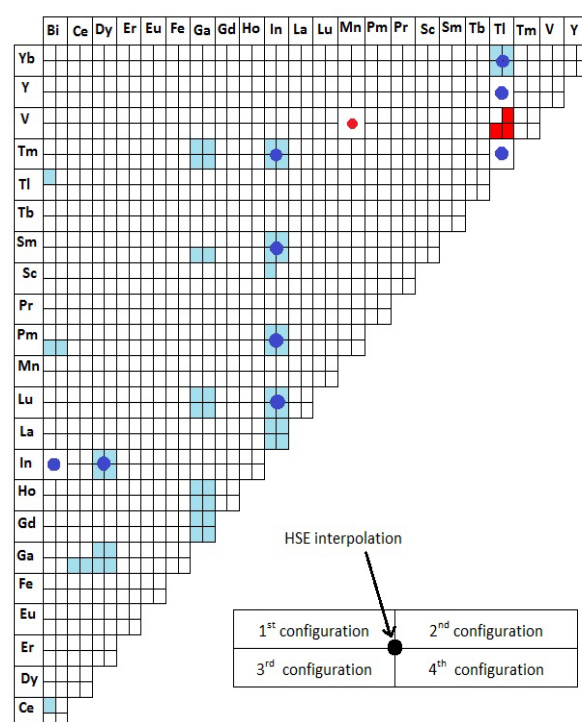


**Fig. 9** Identified 50% ternary oxide TCO candidates  $(A_{0.5}B_{0.5})_2O_3$ . Cell subdivision as in Fig. 6. A filled circle in the center indicates that the three screening criteria are fulfilled within the HSE06 interpolation scheme as well. Blue and red correspond to  $n$ -type and  $p$ -type TCOs, respectively.

than 1 eV (2.5 eV) in the case of PBE (HSE06 interpolation) calculations. Figure 8 illustrates the PBE band alignment of the 50% ternary oxides. For simplicity, in this plot we only consider the oxides for which the most stable (lowest energy) configuration fulfills the three screening criteria.<sup>c</sup> In Fig. 9, all the  $n$ -type and  $p$ -type 50% ternary oxides identified are presented, a colored box indicating that a given configuration fulfills all three criteria within the PBE approach. Thus, in some cases all configurations fulfill the required conditions, while in others only some do so. There is a full circle in the center when the HSE06 interpolation identifies an oxide as a good TCO (there is a single result because the configuration degree of freedom is absent in the interpolation approach). Blue and red indicate  $n$ - and  $p$ -type oxides, respectively.

Similarly, Fig. 10 shows the PBE band alignment of the 25% and 75% alloying  $n$ -type TCO candidates. As mentioned above, one random configuration was considered for these calculations. Figure 11 shows the all the identified 25% and 75%  $n$ - and  $p$ -type TCO candidates, both for the PBE and HSE06 interpolation calculations. Again, blue and red indicate  $n$ - and  $p$ -type oxides, respectively.

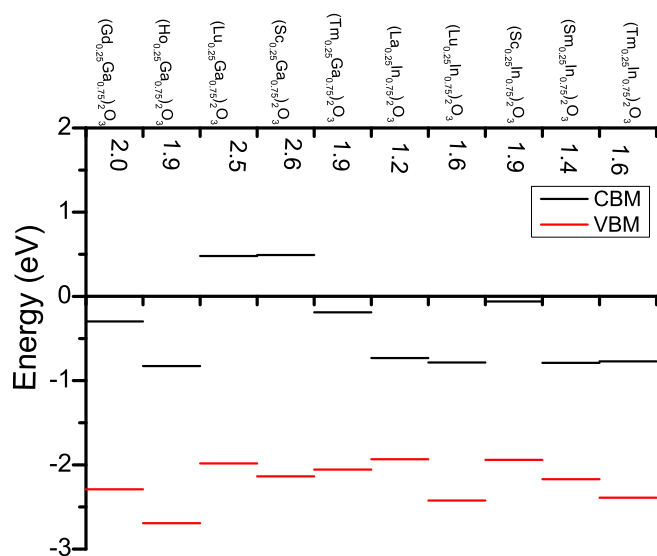


**Fig. 10** The band alignment of the *n*-type 25% ternary compounds from calculations based on the PBE functional. One possible configuration was considered for the calculations.

Examination of Figs. 9 and 11 shows the following. First, considering *n*-type TCOs, none of the oxides containing Er, Eu, Fe, Pr, Mn, or Tb, fulfill all of the three selected criteria, in neither PBE or HSE06 interpolation approaches. On the other hand, there are a few elements that appear repeatedly in the *n*-type TCO ternary candidates. Indeed, it is striking that most of the *n*-type ternary oxides contain Ga and In, independently of the approach (PBE or HSE06 interpolation). Note that the approach based on the PBE functional produces noticeably more 50% alloying TCO candidates than HSE06 interpolation approach. This is not the case for the 25% of 75% alloys.

Turning to the *p*-type ternary oxides, it is interesting that the ternary *p*-type TCO candidates all contain V (cf. Figs. 9 and 11). There are far less candidates than for *n*-type TCOs, whether in the 50% or in the 25% and 75% alloying cases. In the 50% alloying case, the PBE approach produces a single candidate [(Tl<sub>0.5</sub>V<sub>0.5</sub>)<sub>2</sub>O<sub>3</sub>], while the HSE06 interpolation approach produces another single candidate [(Mn<sub>0.5</sub>V<sub>0.5</sub>)<sub>2</sub>O<sub>3</sub>] (cf. Fig. 9). In the 25% alloying case, the PBE approach results in no candidate, while the HSE06 interpolation results in four candidates in the 25% ternaries (cf. Fig. 11). Interestingly, the latter also all contain V.

In order to examine whether the two procedures followed to obtain candidate TCO materials are reliable, we focus on the 50% alloying *n*-type ternaries and proceed as follows. We select those ternaries for which the most stable configuration is indeed a *n*-type TCO candidate according to the PBE procedure, and which at the same time are found to be *n*-type

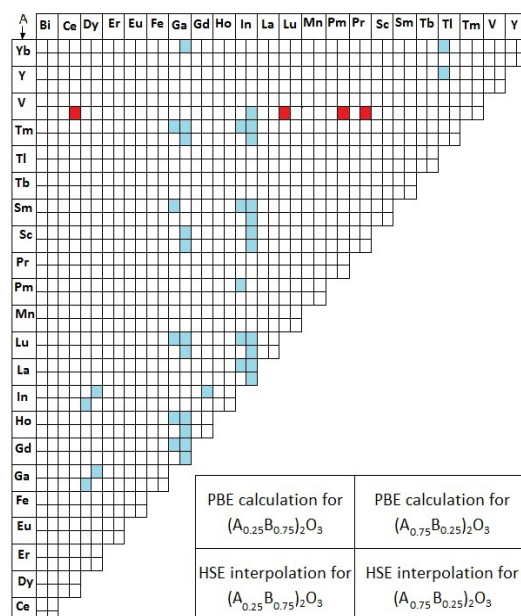


**Fig. 11** Identified potential 25% ( $x=0.75$ ) and 75% ( $x=0.25$ ) ternary oxide TCO candidates ( $A_xB_{1-x}$ )<sub>2</sub>O<sub>3</sub> (one random configuration). Color as in Fig. 9.

candidates with the HSE06 interpolation procedure (cf. Table 2). The reliability of the HSE06 interpolation procedure is, of course, not limited to the 50% alloying cases. We illustrate this by comparing the interpolated band gaps to the HSE06 band gaps for two families of compounds, namely (Dy<sub>x</sub>In<sub>1-x</sub>)<sub>2</sub>O<sub>3</sub> and (Tl<sub>x</sub>Yb<sub>1-x</sub>)<sub>2</sub>O<sub>3</sub>, for  $x = 0, 0.25, 0.5, 0.75$ , and 1. In Table 3 we compare three methods for calculating the band gap: PBE, HSE06, and HSE06 interpolated values of ternary materials. These results indeed show that the interpolated values are very close to those obtained directly from a HSE06 calculation for all values of  $x$ .<sup>a</sup> Moreover, all three methods yield the same trend for the band gap value on changing the composition  $x$ .

The natural step following our present study is to search for suitable dopants, i.e. dopants that act as shallow donors or acceptors in the identified oxides. Furthermore, one must make sure that the doping energy levels are stable against the formation of native defects.<sup>66</sup> Thus, further work is required to identify the impurities that will indeed convert these oxides in good *n*- or *p*-type TCOs.<sup>a</sup>

<sup>a</sup> In a forthcoming publication we discuss in more detail the *p*-type dopability of bixbyite V<sub>2</sub>O<sub>3</sub>.

**Table 2** Comparing band gap and position of the band edges of the most stable configuration of 50% ternary oxides with PBE calculation, HSE calculation, and HSE interpolation results.<sup>†</sup>

AB	band gap(eV)	CBM	VBM
DyIn	2.14	-0.19	-2.32
	3.98	0.69	-3.29
	4.37	0.95	-3.43
InLu	2.08	-0.36	-2.45
	3.97	0.50	-3.47
	4.46	0.92	-3.53
InPm	2.15	-0.04	-2.19
	3.98	0.86	-3.12
	4.26	0.94	-3.32
InSm	2.07	-0.11	-2.19
	3.89	0.75	-3.15
	4.27	0.93	-3.34
InTm	2.18	-0.27	-2.45
	4.07	0.63	-3.44
	4.43	0.92	-3.51
TlYb	1.38	-1.14	-2.51
	2.24	-0.40	-3.44
	3.24	0.14	-3.09

<sup>†</sup> For each oxide, 1<sup>st</sup>, 2<sup>nd</sup>, and 3<sup>rd</sup> row of data refer to PBE calculation, HSE calculation, and HSE interpolation results.

## 4 Conclusion

We present a density-functional based computational high-throughput scheme to screen a class of oxides in order to find new candidate TCO materials. The high-throughput method presented here can be easily applied to different classes of materials. Here, we screen the electronic properties of 1541 bixbyite oxides, 23 binaries and 1518 ternaries (binary alloys). The oxides are screened to ensure (i) a minimum band gap, guaranteeing a reasonable transparency in the visible, (ii) a minimum thermodynamic phase stability, and (iii) a positioning of the charge neutrality level in the band gap indicating easy *n*- or *p*-type dopability. Among the binaries, our calculations yield  $V_2O_3$ , a relatively simple system with a band gap of 2.4 eV, as an interesting possible *p*-type TCO. Our results indicate  $Ga_2O_3$  as a *n*-type candidate, besides  $In_2O_3$ . Among the ternaries, it is remarkable that most of the *n*-type candidates contain either Ga or In, while the *p*-type candidates all contain V. Focusing on the 50% alloys, a more robust short list of *n*-type candidates is produced by comparing the results of our two screening approaches with full HSE06 calculations. The promising candidates thus identified, most of them with a band gap larger than 3 eV, are given by  $(A_{0.5}B_{0.5})_2O_3$  with AB=(DyIn, InLu, InSm, InTm).<sup>a</sup>

Further research should identify the type of dopants that can

<sup>a</sup> Although  $(In_{0.5}Pm_{0.5})_2O_3$ , and  $(Tl_{0.5}Yb_{0.5})_2O_3$  are in Table 2, we do not include them in the final list because Pm is radioactive, and Tl is toxic.

**Table 3** Comparing band gap of  $(Dy_xIn_{1-x})_2O_3$ , and  $(Tl_xYb_{1-x})_2O_3$  with PBE calculation, HSE calculation, and HSE interpolation results.

compound	$E_{g,PBE}$	$E_{g,HSE}$	$E_{g,HSEinterpolation}$
$In_2O_3$	0.93	2.85	2.85
$(Dy_{0.25}In_{0.75})_2O_3$	1.57	3.44	3.61
$(Dy_{0.5}In_{0.5})_2O_3$	2.14	3.98	4.37
$(Dy_{0.75}In_{0.25})_2O_3$	2.27	4.26	5.13
$Dy_2O_3$	3.94	5.90	5.90
$Tl_2O_3$	0.01	0.44	0.44
$(Tl_{0.75}Yb_{0.25})_2O_3$	0.46	1.67	1.83
$(Tl_{0.5}Yb_{0.5})_2O_3$	1.38	2.24	3.23
$(Tl_{0.25}Yb_{0.75})_2O_3$	2.25	3.09	4.63
$Yb_2O_3$	3.4	6.04	6.04

effectively bring about these systems as TCOs.

## 5 Acknowledgement

We gratefully acknowledge financial support from the IWT-Vlaanderen through the ISIMADE project(IWT-n 080023), the FWO-Vlaanderen through project G.0150.13 and a GOA fund from the University of Antwerp. This work was carried out using the HPC infrastructure of the University of Antwerp (CalcUA) a division of the Flemish Supercomputer Center VSC, which is funded by the Hercules foundation and the Flemish Government (EWI Department).

## References

- 1 R. G. Gordon, *MRS Bulletin*, 2000, **25**, 52.
- 2 E. Fortunato, D. Ginley, H. Hosono and D. C. Paine, *MRS Bulletin*, 2007, **32**, 242.
- 3 D. Morgan, G. Ceder and S. Curtarolo, *Meas. Sci. Technol.*, 2005, **16**, 296.
- 4 Y. Wu, P. Lazic, G. Hautier, K. Persson and G. Ceder, *Energy Environ. Sci.*, 2013, **6**, 157.
- 5 S. Curtarolo, G. L. W. Hart, M. B. Nardelli, N. Mingo, S. Sanvito and O. Levy, *Nature Mater.*, 2013, **12**, 191–201.
- 6 K. Yang, W. Setyawan, S. Wang, M. B. Nardelli and S. Curtarolo, *Nature Mater.*, 2012, **11**, 614–619.
- 7 R. Armiento, B. Kozinsky, M. Fornari, and G. Ceder, *Phys. Rev. B*, 2011, **84**, 014103.
- 8 G. K. H. Madsen, *J. Am. Chem. Soc.*, 2006, **128**, 12140.
- 9 G. Hautier, A. Miglio, G. Ceder, G.-M. Rignanese and X. Gonze, *Nature Commun.*, 2013, **4**, 2292.
- 10 P. Hohenberg and W. Kohn, *Phys. Rev.*, 1964, **136**, B864.
- 11 W. Kohn and L. J. Sham, *Phys. Rev. B*, 1965, **140**, A1133.
- 12 G. Kresse and J. Hafner, *Phys. Rev. B*, 1993, **47**, R558.
- 13 G. Kresse and J. Hafner, *J. Phys. Cond. Matt.*, 1994, **6**, 8245.
- 14 G. Kresse and J. Furthmüller, *Comput. Mater. Sci.*, 1996, **6**, 15.
- 15 G. Kresse and J. Furthmüller, *Phys. Rev. B*, 1996, **54**, 11169.
- 16 G. Kresse and D. Joubert, *Phys. Rev. B*, 1999, **59**, 1758.
- 17 P. E. Blöchl, *Phys. Rev. B*, 1994, **50**, 17953.
- 18 J. P. Perdew, K. Burke and M. Ernzerhof, *Phys. Rev. Lett.*, 1996, **77**, 3865.

- 19 J. Heyd, G. E. Scuseria and M. Ernzerhof, *J. Chem. Phys.*, 2003, **118**, 8207.
- 20 A. V. Krukau, O. A. Vydrov, A. F. Izmaylov and G. E. Scuseria, *J. Chem. Phys.*, 2006, **125**, 224106.
- 21 H. Xiao, J. Tahir-Kheli and W. A. Goddard, *J. Phys. Chem. Lett.*, 2011, **2**, 212.
- 22 H. J. Monkhorst and J. D. Pack, *Phys. Rev. B*, 1976, **13**, 5188.
- 23 K. L. Chopra, S. Major and D. K. Pandya, *Thin Solid Films*, 1983, **102**, 1.
- 24 K. A. Johnson and N. W. Ashcroft, *Phys. Rev. B*, 1998, **58**, 15548.
- 25 C. S. Wang and W. E. Pickett, *Phys. Rev. Lett.*, 1983, **51**, 597.
- 26 T. M. Henderson, J. Paier and G. E. Scuseria, *Phys. Status Solidi B*, 2011, **248**, 767.
- 27 A. Schleife, F. Fuchs, C. Rödl, J. Furthmüller and F. Bechstedt, *Appl. Phys. Lett.*, 2009, **94**, 012104.
- 28 P. Deák, B. Aradi and T. Frauenheim, *J. Phys. Chem. C*, 2011, **115**, 3443.
- 29 B. Höfiling, A. Schleife, F. Fuchs, C. Rödl and F. Bechstedt, *Appl. Phys. Lett.*, 2010, **97**, 032116.
- 30 S.-H. Wei, *Comput. Mater. Sci.*, 2004, **30**, 337.
- 31 A. Walsh, Y. Yan, M. M. Al-Jassim and S.-H. Wei, *J. Chem. Phys.*, 2008, **112**, 12044.
- 32 Y. Bréard, H. Fjellvåg and B. Hauback, *Solid State Commun.*, 2011, **151**, 223–226.
- 33 H. H. Tippins, *J. Phys. Chem. Solids*, 1966, **27**, 1069.
- 34 J. R. Rustad, *Am. Mineral.*, 2012, **97**, 791.
- 35 D. R. Lide, *Handbook of Chemistry and Physics*, CRC Press, 84th edn., 2004.
- 36 D. Weber, A. Stork, S. Nakhla, C. Wessel, C. Reimann, W. Hermes, A. Müller, T. Ressler, R. Pöttgen, T. Bredow, R. Dronskowski and M. Lerch, *Inorg. Chem.*, 2011, **50**, 6762.
- 37 A. Bergerud, R. Buonsanti, J. L. Jordan-Sweet and D. J. Milliron, *Chem. Mater.*, 2013, **25**, 3172.
- 38 C. M. Julien, M. Massot and C. Poinson, *Spectrochim. Acta Mol. Biomol.*, 2004, **60**, 689.
- 39 L. Ben-Dor, E. Fischbein and Z. Kalman, *Acta Cryst. B*, 1976, **32**, 667.
- 40 S. Yoshioka, H. Hayashi, A. Kuwabara, F. Oba, K. Matsunaga and I. Tanaka, *J. Phys. Cond. Matt.*, 2007, **19**, 346211.
- 41 Ž. Antić, R. Krsmanović, Wojtowicz, E. Zych, B. Bártoová and M. D. Dramićanin, *Opt. Mater.*, 2010, **32**, 1612.
- 42 P. W. Peacock and J. Robertson, *J. Appl. Phys.*, 2002, **92**, 4712.
- 43 G. Wilk and R. M. Wallace, *MRS Bulletin*, 2002, **27**, 186.
- 44 L. Marsella and V. Fiorentini, *Phys. Rev. B*, 2004, **69**, 172103.
- 45 A. Bourlange, D. J. Payne, R. G. Egdell, J. S. Foord, P. P. Edwards, M. O. Jones, A. Schertel, P. J. Dobson and J. L. Hutchison, *Appl. Phys. Lett.*, 2008, **92**, 092117.
- 46 A. Walsh, J. L. F. D. Silva, S. Wei, C. Körber, A. Klein, L. F. J. Piper, A. DeMasi, K. E. Smith, G. Panaccione, P. Torelli, D. J. Payne, A. Bourlange and R. G. Egdell, *Phys. Rev. Lett.*, 2008, **100**, 167402.
- 47 P. D. C. King, T. D. Veal, F. Fuchs, C. Y. Wang, D. J. Payne, A. Bourlange, H. Zhang, G. R. Bell, V. Cimalla, O. Ambacher, R. G. Egdell, F. Bechstedt and C. F. McConville, *Phys. Rev. B*, 2009, **79**, 205211.
- 48 I. Tanaka, K. Tatsumi, M. Nakano and H. Adachi, *J. Am. Ceram. Soc.*, 2002, **85**, 68.
- 49 S. Lany and A. Zunger, *Phys. Rev. Lett.*, 2011, **106**, 069601.
- 50 G. y. Adachi and N. Imanaka, *Chem. Rev.*, 1998, **98**, 1479.
- 51 A. F. Andreeva, I. Y. Gilman and Z. Prikl, *Spectrosc.*, 1978, **28**, 895.
- 52 H. Jiang, R. I. Gomez-Abal, P. Rinke and M. Scheffler, *Phys. Rev. Lett.*, 2009, **102**, 126403.
- 53 W. B. White, *Appl. Spectrosc.*, 1967, **21**, 167.
- 54 G. Concas, J. K. Dewhurst, A. Sanna, S. Sharma and S. Massidda, *Phys. Rev. B*, 2011, **84**, 014427.
- 55 M. Badylevich, S. Shamuilia, V. V. Afanas'ev and A. Stesmans, *Appl. Phys. Lett.*, 2007, **90**, 252101.
- 56 A. I. Shelykh, A. V. Prokofiev and B. T. Melekh, *Fiz. Tverd. Tela (St. Petersburg)*, 1996, **38**, 427.
- 57 A. W. Carbonari, J. Mestnik-Filho, R. N. Attili, M. Moralles and R. N. Saxena, *Hyperfine Interact.*, 1999, **120**, 475.
- 58 A. B. Kehoe, D. O. Scanlon and G. W. Watson, *Phys. Rev. B*, 2011, **83**, 233202.
- 59 A. Matsumoto, Y. Koyama and I. Tanaka, *Phys. Rev. B*, 2010, **81**, 094117.
- 60 P. Reunchan, X. Zhou, S. Limpijumnong, A. Janotti and C. G. Van de Walle, *Current Appl. Phys.*, 2011, **11**, S296.
- 61 J. B. Varley, J. R. Weber, A. Janotti and C. G. V. de Walle, *Appl. Phys. Lett.*, 2010, **97**, 142106.
- 62 K. Held, G. Keller, V. Eyert, D. Vollhardt and V. I. Anisimov, *Phys. Rev. Lett.*, 2001, **86**, 5345.
- 63 G. A. Thomas, D. H. Rapkine, S. A. Carter, A. J. Millis, T. F. Rosenbaum, P. Metcalf and J. M. Honig, *Phys. Rev. Lett.*, 1994, **73**, 1529.
- 64 C. Wessel, C. Reimann, A. Müller, D. Weber, M. Lerch, T. Ressler, T. Bredow and R. Dronskowski, *J. Comput. Chem.*, 2012, **33**, 2102.
- 65 L. Vegard, *Z. Phys. B*, 1921, **5**, 17.
- 66 J. Robertson and S. J. Clark, *Phys. Rev. B*, 2011, **83**, 075205.